A&A 392, 329–334 (2002)
DOI: 10.1051/0004-6361:20020945
© ESO 2002

Astronomy & Astrophysics

Solar differential rotation determined by tracing coronal bright points in SOHO-EIT images

II. Results for 1998/99 obtained with interactive and automatic methods

R. Brajša[1,2,⋆], H. Wöhl[1], B. Vršnak[2], V. Ruždjak[2], F. Clette[3], and J.-F. Hochedez[3]

[1] Kiepenheuer-Institut für Sonnenphysik (KIS), Schöneckstr. 6, 79104 Freiburg, Germany
e-mail: hw@kis.uni-freiburg.de
[2] Hvar Observatory, Faculty of Geodesy, University of Zagreb, Kačićeva 26, 10000 Zagreb, Croatia
e-mail: romanb@geodet.geof.hr; bvrsnak@geodet.geof.hr; vruzdjak@geodet.geof.hr
[3] Observatoire Royal de Belgique (ORB), Av. Circulaire 3, 1180 Bruxelles, Belgium
e-mail: Frederic.Clette@oma.be; hochedez@oma.be

Received 15 April 2002 / Accepted 6 June 2002

Abstract. Full-disc solar images obtained with the Extreme Ultraviolet Imaging Telescope (EIT) on board the Solar and Heliospheric Observatory (SOHO) were used to analyse solar differential rotation by tracing coronal bright points. The results obtained with the interactive and the automatic method for the time period June 4, 1998 to May 22, 1999 are presented and compared. A possible north–south rotational asymmetry and differences in the rotation velocity curves for various subtypes of tracers are investigated.

Key words. Sun: corona – Sun: UV radiation – Sun: rotation

1. Introduction

There are many indications of north–south asymmetry of the solar magnetic activity (e.g., Carbonell et al. 1993; Oliver & Ballester 1994; Vernova et al. 2002). Coronal bright points are magnetic tracers, and it would be interesting to search for a possible north–south asymmetry of the solar rotation determined by them. The sizes of coronal bright points are 15–30 arcsec (Golub et al. 1974; Harvey-Angle 1993) or more (Golub & Pasachoff 1997) and their lifetimes are 2–48 hours (Skylab observations). The lower limits on the size and lifetime of coronal bright points were instrumentally determined, while the upper limits were arbitrarily chosen to separate them from active regions. Measurements performed later on with the Yohkoh, SOHO, and TRACE spacecrafts enabled identification of coronal transient brightenings also on smaller size and time scales (e.g., Shimizu et al. 1994; Koutchmy et al. 1997; Krucker et al. 1997; Berghmans et al. 2001; Brković et al. 2001). Coronal bright points consist of several small loops and observations performed with a high spatial and temporal resolution reveal their subtle structural changes in some cases (Brown et al. 2001). Coronal bright points can sometimes form large-scale patterns in the solar corona, called large-scale emitting chains (Chertok 1999, 2001).

This paper continues our analysis of the solar differential rotation determined with coronal EUV bright points as tracers. The interactive and the automatic methods of data reduction were described by Brajša et al. (2001a) (hereafter Paper I), where also some test-results obtained with the two methods were presented and compared. The two methods were further refined by Brajša et al. (2001b) (hereafter Paper II) and by Wöhl et al. (2001) (hereafter Paper III) and applied to data sets from different time intervals within the period June 4, 1998 to May 22, 1999. In Papers II and III preliminary results obtained by various observers and for different data subsets were presented and the analysis described therein provided a homogenous set of results embracing all available data for the time period 1998/99. These results include the mean latitude and Central Meridian Distance (CMD), rotational and meridional velocity, as well as the tracing time and tracer subtype for each identified bright point. Tracers were divided into three subtypes including point-like structures, small loops, and small active regions, taking into account morphological characteristics of coronal bright points reported earlier. In this paper the results obtained applying the interactive and the automatic method are compared. Furthermore, a possible north–south rotational asymmetry, as well as the differences in the rotation velocity curves for various subtypes of tracers are investigated and discussed.

Send offprint requests to: R. Brajša,
e-mail: rbrajsa@kis.uni-freiburg.de
⋆ Alexander von Humboldt Research Fellow at KIS.

Article published by EDP Sciences and available at http://www.aanda.org or http://dx.doi.org/10.1051/0004-6361:20020945

2. The data set and reduction methods

About 600 full-disc solar filtergrams in the Fe XV line at the wavelength of 28.4 nm provided by the EIT instrument on board SOHO were analysed. The observations cover the period June 4, 1998 to May 22, 1999, with some interruptions. Usually 4 images per day, i.e., one image every 6 hours were taken, but occasionally there are gaps of 12 hours or more between the successive images. The orientation of the solar rotation axis in some images was not aligned with the $y-$axis of the image. Although test reductions were performed including such images, they were excluded from the present analysis. Further, a few images were not usable because of many missing telemetry blocks. More details about availability of data and image selection were given in Paper I. The number of images actually analysed was reduced to 463; they were taken in June, November, and December 1998 and in March, April, and May 1999 (for details see Paper II). All images were preprocessed correcting the defects (grid, CCD flat field) and the CCD offset. However, the preprocessing of images did not include corrections of in-flight degradations.

The interactive method of data reduction is based on the visual identification of tracers and was described in detail in Papers I and II. The bright points are identified in sequences of images on the computer screen and their persistence in consecutive images at approximately the same latitude and shifted along the CMD is checked. The tracing of bright points applying the interactive method was performed by several observers independently.

The automatic method of data reduction relies on the IDL procedure "Regions Of Interest (ROI) segmentation" and was described in detail in Papers I and III. The ROI parameters that can be preset are the sharpness of the subimages (s), their circumference range (c) and the intensity range of their brightness (i). In the present work the following ROI parameters are used: s was limited from 30 to 255 relative units, c was in the range 30 to 80 EIT pixels (78.9 to 210.3 arcsec) and i was limited to 100 to 600 relative intensity units. The centres of the selected subimages were automatically traced in triplets of consecutive full-disc solar images taken every 6 hours; the last image in a triplet was the first one in the next triplet. Sequences of images taken 12 or 18 hours apart were not used here, contrary to the interactive method, when this sometimes occured. In the automatic method the numerically allowed latitudinal variation of the traced feature was 1 degree (from one image to the next).

The improved solar disc coordinates (the solar radius and the position of the solar disc centre in EIT pixels) provided by Auchère et al. (1998) were used in the coordinate transformation as discussed in Paper I. This is indicated in the present paper by "nc" in all figures. The rotational velocity was determined using a linear least squares fit of CMD as a function of time for tracers identified either with the interactive or with the automatic method. The time-dependent transformation from the synodic to the sidereal rotational velocity was performed taking into account the variable velocity of the Earth and SOHO in their orbits around the Sun (e.g., Roša et al. 1995; Brajša et al. 2002).

As usual, the solar differential rotation is represented by

$$\omega(b) = A + B\sin^2 b + C\sin^4 b, \quad (1)$$

where ω is the sidereal angular rotation velocity in degrees per day [$^\circ$ d^{-1}], b is the heliographic latitude [$^\circ$], and A, B, and C are the parameters of the differential rotation curve. In this paper only the first two terms in Eq. (1) are taken into account as a first approximation, since only results within our data set will be presented and compared. The third term in Eq. (1) will be important in a later paper when a comparison with other data sets and methods will be performed.

The exclusion of the extreme rotation velocity values was carried out in two steps. All sidereal rotation velocities lower than 8° d^{-1} and higher than 18° d^{-1} were excluded regardless of the tracer's latitude. Then the rotation velocity parameters from Eq. (1) were found for all remaining data points. Further, a filter excluding all velocity values differing by $\delta = 2.0^\circ$ d^{-1} or more from the mean curve was applied to the data and finally new parameters were calculated. More details about the velocity filter and numbers of data points in different subsets before applying it are given in Papers I–III.

Finally we point out that the data reduction procedures used here are a little bit different from the ones described earlier in Paper I, as a result of additional experience, as described in Papers II and III. In particular, the adjustable ROI parameters c and i were selected in such a way that the automatic method resembles as much as possible the interactive one, as discussed in Paper III. Further, a refined two-step filter on rotation velocity is applied here equivalently for the two methods of data reduction.

3. Results

3.1. Observational characteristics of bright points

We first briefly summarize the morphological characteristics of the three subtypes of coronal bright points used as tracers in our observations performed with the interactive method. The point-like structures have sizes generally less than 15 arcsec in diameter. The small loops are elongated structures less than 15 arcsec wide and up to 50 arcsec long having a loop-like structure. Finally, the small active regions are more or less round structures having discernible bright surfaces with diameters up to approximately 50 arcsec. Structural changes were sometimes observed during the tracing time. In such cases, the tracer subtype label was ascribed according to the morphological characteristics observed most often during the tracing. When such structural and evolutionary changes were observed, they often occured on time scales less then 18 hours. We point out that various observers sometimes ascribed different subtypes to the same structure, i.e., in a certain fraction of events the decision depended on personal judgement. Finally, in at least one case a large-scale chain formed by coronal bright points was observed. It was persistent in a number of subseqent images. Similar morphological characteristics of coronal bright points were also reported in the literature, as described in Sect. 1.

Table 1. Differential rotation parameters A and B from Eq. (1) for the data set 1 (tracing intervals up to 11 images) obtained applying the interactive method. The sidereal parameters and their standard errors (M) expressed in $^\circ$ d^{-1} for the complete data set and for both solar hemispheres separately, as well as for the three tracer subtypes are presented. n – the number of tracers, lat – the latitude range [°], R – remark, N – north, S – south, PLS – point-like structure, SL – small loop, SAR – small active region.

$A \pm M_A$	$-B \pm M_B$	n	lat	R
14.59 ± 0.03	3.18 ± 0.10	1179	0.1–70.1	N+S, all
14.55 ± 0.04	2.95 ± 0.15	545	0.1–67.4	N, all
14.64 ± 0.04	3.44 ± 0.15	635	0.1–70.1	S, all
14.51 ± 0.04	3.26 ± 0.15	534	0.6–67.4	N+S, PLS
14.63 ± 0.07	3.62 ± 0.26	197	0.3–70.1	N+S, SL
14.64 ± 0.04	2.78 ± 0.18	450	0.1–67.4	N+S, SAR

3.2. Interactive method

The preliminary results obtained with the interactive method are presented separately for data reductions performed by five independent observers in Paper II. However, no observer covered all of the six time subintervals within the analysed time period June 4, 1998 to May 22, 1999, although each subinterval was treated by at least two observers independently. So, a homogeneous data set covering each time interval once, using results of different observers, was formed. The observers applied the interactive method in two different manners with respect to the tracing time. Some of them confined the tracing times to shorter intervals, while others traced the bright points as long as possible. In this way two homogeneous data sets were obtained: The "data set 1" (tracers were followed in up to 11 images) and the "data set 2" (tracers were followed in up to 24 images).

In Tables 1 and 2 the results obtained with the interactive method are presented for data sets 1 and 2, respectively. Solar differential rotation parameters from Eq. (1) are presented together with their errors, the number of tracers used and the latitude ranges. The results are presented for the complete data sets, for the northern and the southern solar hemispheres separately, as well as distinguishing the three tracer subtypes. These additional constraints were applied before the filtering, and all presented results were calculated after the two-step filtering, as described earlier. As an example, the results for the data set 1, obtained for the southern solar hemisphere, are presented in Fig. 1.

3.3. Automatic method

The preliminary results of the automatic method were presented separately for the six subintervals within the period June 4, 1998 to May 22, 1999 in Paper III. Here we present the results for the complete data set combined together from these six subsets. In Table 3 the results of the automatic method are presented in a similar way as Tables 1 and 2 for the interactive method. However, the identification of the tracer subtype was not possible in the case of the automatic method. In Fig. 2 the results for both solar hemispheres treated together are presented as an example.

Table 2. As Table 1 for the data set 2 (tracing intervals up to 24 images).

$A \pm M_A$	$-B \pm M_B$	n	lat	R
14.60 ± 0.03	3.31 ± 0.12	919	0.1–68.8	N+S, all
14.57 ± 0.05	3.34 ± 0.18	417	0.1–67.4	N, all
14.63 ± 0.04	3.36 ± 0.15	503	0.1–68.8	S, all
14.54 ± 0.06	3.25 ± 0.20	345	0.1–67.4	N+S, PLS
14.63 ± 0.06	3.64 ± 0.21	240	0.7–68.8	N+S, SL
14.64 ± 0.05	3.18 ± 0.21	336	0.1–66.2	N+S, SAR

Table 3. Similar as Tables 1 and 2 for the automatic method.

$A \pm M_A$	$-B \pm M_B$	n	lat	R
14.53 ± 0.03	2.68 ± 0.13	1500	0.1–71.0	N+S
14.51 ± 0.05	2.51 ± 0.20	723	0.1–69.4	N
14.54 ± 0.04	2.80 ± 0.17	781	0.1–71.0	S

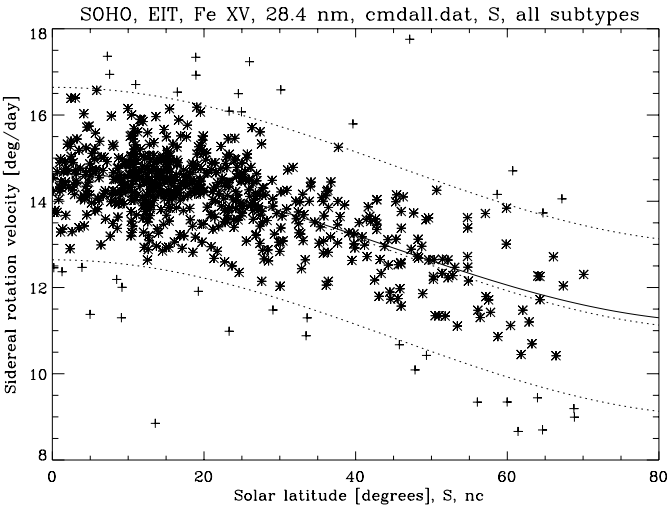

Fig. 1. Sidereal rotation velocities determined tracing coronal bright points with the interactive method for the southern solar hemisphere using the data set 1. The data points excluded by the second filter, as described in Sect. 2, are shown by crosses. The fitted differential rotation curve using all data points presented here and the error ranges of 2° d^{-1} are denoted by dotted lines. The full line gives the differential rotation curve of the filtered data (stars). It is defined by the differential rotation parameters given in the third line of Table 1.

4. Discussion

4.1. Comparison of the two methods

The results of the interactive method are very similar for data sets 1 and 2 (Tables 1 and 2 and Fig. 3) in spite of the difference in tracing time. Note that the y–axis in Figs. 3–8 is stretched by a factor of 2.5 in comparison to Figs. 1 and 2. On the other hand the differential character of rotation is less pronounced

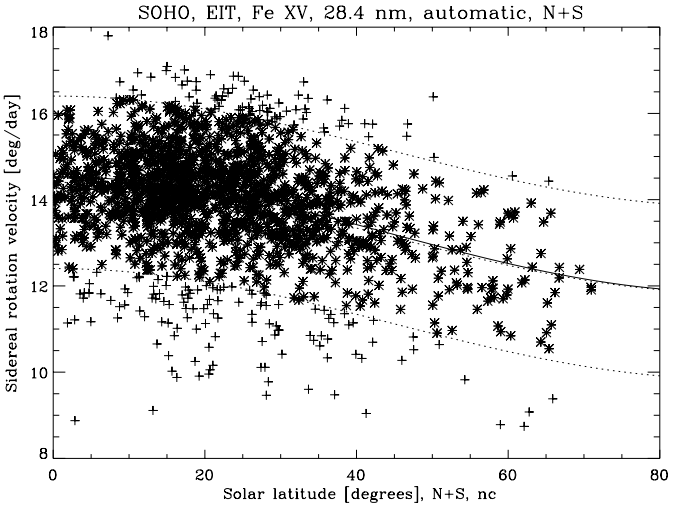

Fig. 2. The results of the automatic method applied to the complete data set (both solar hemispheres treated together) are presented in an analogous way as in Fig. 1. Fit parameters are given in the first line in Table 3.

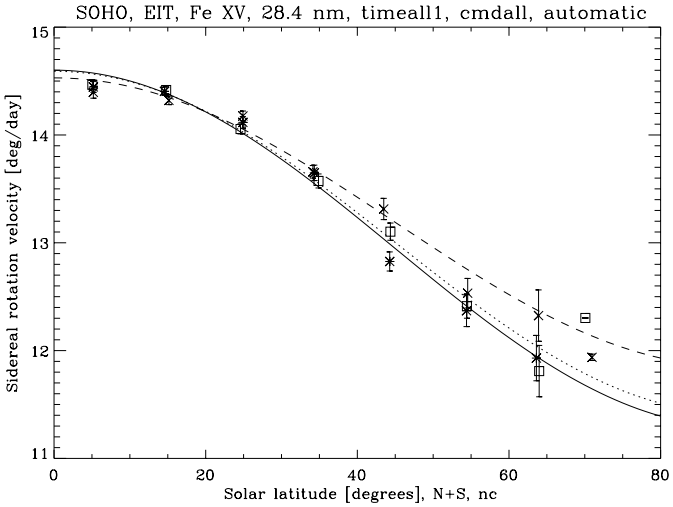

Fig. 3. Mean values of sidereal rotation velocities obtained using the interactive method for the data set 1 (squares and dotted line) and for the data set 2 (stars and full line), and the ones obtained using the automatic method (crosses and dashed line). The averaging is performed in 10° latitude bins and the error bars indicate the standard errors of the means in each bin. The error bars at latitudes above 70° are not reliable, since just a single data point or a couple of them with very similar values within the bins were averaged. Both solar hemispheres are treated together. The lines represent least-squares fits to all filtered data points in each data set (e.g., Fig. 2). The parameters are given in first lines in Tables 1–3.

in results of the automatic method than in those of the interactive method (Fig. 3). The difference in the parameter B for the two methods is statistically significant at the 2σ level (first rows in Tables 1–3). The parameter B defines the differentiality/rigidity of the solar rotation curve. The differential rotation curve determined by tracing sunspots lies approximately between the rotational profiles of coronal bright points obtained with the automatic and interactive methods, respectively.

An explanation for this rigid component of the solar rotation determined by tracing coronal bright points with the automatic method is the possibility that in some cases parts of large active regions were identified and traced. In applying the interactive method this was not the case because of the visual identification of tracers, which enables one to distinguish isolated structures on smaller scales. Ordinary active regions appear in EUV often very large, blending significant portions of the solar disc. Another possibility would be that the automatic method systematically favors bright points inside coronal holes because of sharper contrast in these regions.

In some cases active regions may form large-scale patterns, i.e., complexes of activity (Gaizauskas et al. 1983). Large-scale and long-lived tracers reveal in general a more rigid character of rotation than small-scale and short-lived ones having a more differential rotation velocity (Stix 1989). Both types of rotation may be present at the same latitude bands and one interpretation of the rigid component was in the framework of the magnetic flux-transport model (Sheeley et al. 1987; Wang & Sheeley 1994). This model was also used to investigate the rigid component in the rotation of coronal holes (Nash et al. 1988). It is also interesting to note that some large-scale emitting chains formed by coronal bright points were cospatial with the boundaries of coronal holes (Chertok 1999, 2001).

4.2. North–south asymmetry of the rotation

The north–south asymmetry of solar rotation determined by tracing coronal bright points is generally small and not significant (Tables 1–3, Figs. 4–6). The differences in the rotation parameters A and B for the northern and southern solar hemispheres are statistically significant on the 1σ level only for the data set 1 (Table 1), and are below the 1σ level in other cases (Tables 2 and 3). However, it is interesting that in case of the data set 1 and for the automatic method (Figs. 4 and 6, respectively) the southern solar hemisphere had a more differential character of rotation than the northern one, implying a somewhat slower rotation at high southern latitudes in comparison with the northern ones.

It is not uncommon that coronal features reveal a north–south rotational asymmetry (e.g., Hoeksema & Scherrer 1987; Nash 1991). However, the north–south rotational asymmetry determined here by tracing coronal bright points is small and not significant, although in two out of the three cases the northern solar hemisphere, at high latitudes, rotated a little bit faster than the southern one, as earlier described. This is in a qualitative agreement with the north–south rotational asymmetry of the photospheric magnetic field (Antonucci et al. 1990) and with the north–south asymmetry of the solar rotation determined by tracing microwave low brightness temperature regions (Brajša et al. 2000).

4.3. Rotation velocity for various tracer subtypes

The differential rotation curves for various subtypes of coronal bright points observed with the interactive method is presented for data sets 1 and 2 in Figs. 7 and 8, respectively. In both data sets small active regions reveal on average the highest and most rigid differential rotation in comparison with the

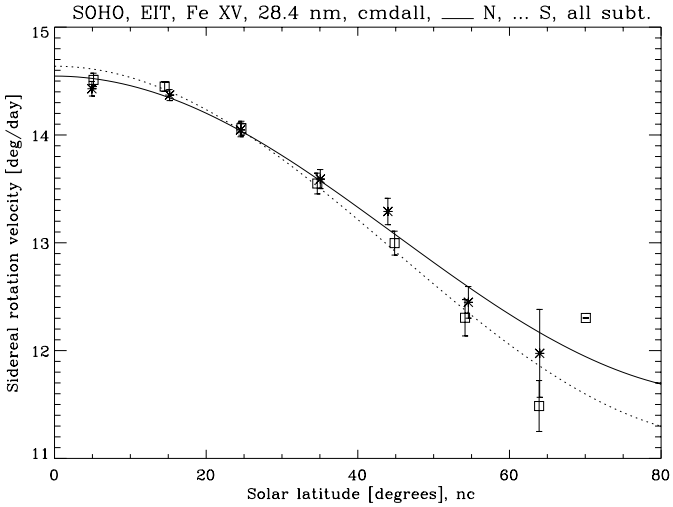

Fig. 4. Comparison of rotation in the northern and the southern solar hemispheres presented in an analogous way as in Fig. 3. The results for the northern solar hemisphere are represented by stars and the full line and for the southern one by squares and the dotted line (interactive method, data set 1, see fit parameters in Table 1).

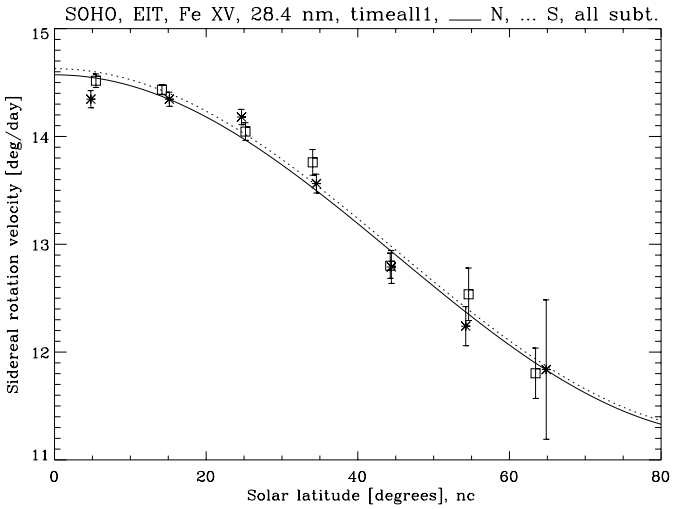

Fig. 5. As Fig. 4 for the data set 2 (Table 2).

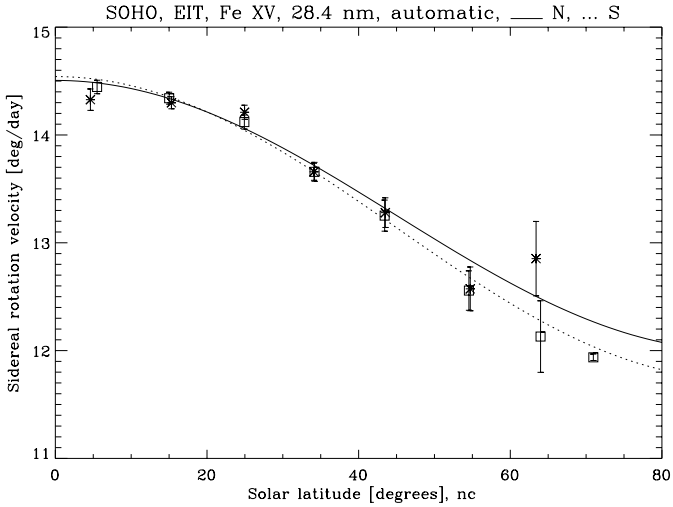

Fig. 6. As Fig. 4 for the automatic method (Table 3).

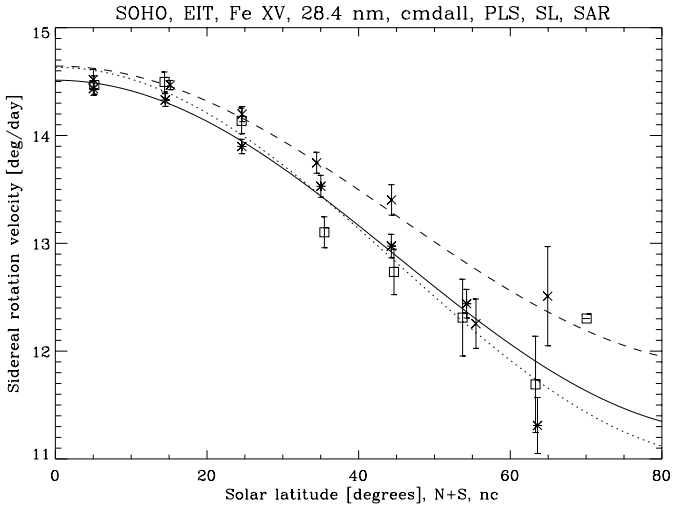

Fig. 7. Similar as Fig. 3 for the three tracer subtypes (interactive method, data set 1, for fit parameters see Table 1). Point-like structures are indicated by stars and the full line, small loops by squares and the dotted line, and small active regions by crosses and the dashed line.

point-like structures and small loops. The differences in the rotation parameter B are largest between the small loops and small active regions. This difference is statistically significant at almost the 2σ level in the data set 1 (Table 1) and slightly above the 1σ level in the data set 2 (Table 2). We also note that in the case of the data set 1 the small loops and the small active regions have a higher equatorial rotation velocity than the point-like structures. The differences in the rotation parameter A are statistically significant at the 1σ level (Table 1).

We can try to understand the rigid component in rotation of small active regions, as compared with the other two tracer subtypes, using a similar argument as in the case of the results obtained with the automatic method (Sect. 4.1). Larger structures have less differential rotation. Another possibility is the projection effect (Vršnak et al. 1999) due to a larger height of small active regions in comparison with the other two tracer subtypes. Finally, we would like to stress that the tracers used in this analysis are dissipative phenomena belonging to the lower corona. This should be taken into account when comparing obtained differential rotation profiles among themselves and with other results.

5. Conclusions

In this paper an analysis of the solar differential rotation is performed by tracing coronal EUV bright points. The interactive and the automatic method are applied to the period June 4, 1998 to May 22, 1999. Both methods were further developed and refined in comparison with Paper I. The north–south rotational asymmetry of coronal bright points is small and statistically not significant, although qualitatively consistent with some other reports. The solar differential rotation curve determined with the automatic method is on average more rigid than the one determined with the interactive method. Similarly, small active regions have a more rigid differential rotation than

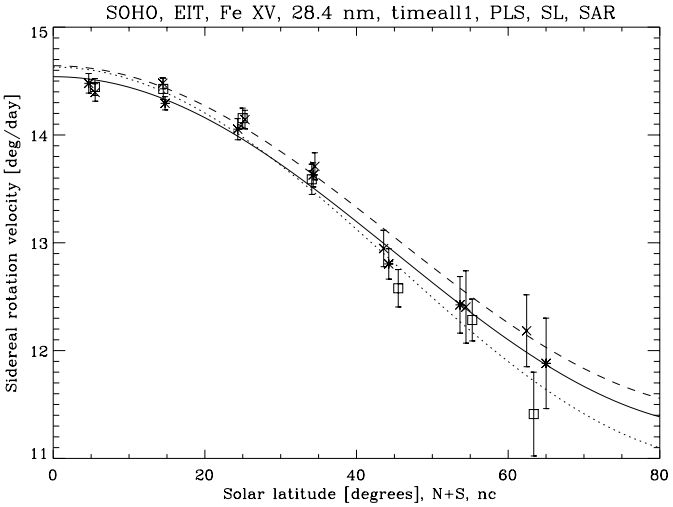

Fig. 8. As Fig. 7 for the data set 2 (Table 2).

point-like structures and small loops. These results are interpreted in terms of the dependence of differentiality/rigidity of solar rotation on the tracer sizes and heights, as well as on their possible connections to complexes of activity, coronal holes and large-scale emitting chains.

Using data sets prepared within this paper, we will analyse the number and velocity distributions of coronal bright points, their lifetimes and their height correction in subsequent papers. Further, a comparison with other results on solar rotation, especially obtained tracing sunspots, will be performed and properties of the coronal bright points velocity field will be studied.

Acknowledgements. This work was performed with the support of the Alexander von Humboldt Foundation and is related to the SOHO-EIT Proposal Brajsa_206. SOHO is a project of international cooperation between ESA and NASA. We would like to thank the EIT team for developing and operating the instrument. Further, we would like to thank the students T. J. Schuck, K. Schawinski-Guiton, and A. Wegner for taking part in the data reduction performed with the interactive method. Finally, F. Clette and J.-F. Hochedez acknowledge the support from the Belgian OSTC and from Prodex.

References

Antonucci, E., Hoeksema, J. T., & Scherrer, P. H. 1990, ApJ, 360, 296
Auchère, F., Boulade, S., Koutchmy, S., et al. 1998, A&A, 336, L57
Berghmans, D., McKenzie, D., & Clette, F. 2001, A&A, 369, 291
Brajša, R., Ruždjak, V., Vršnak, B., et al. 2000, Sol. Phys., 196, 279
Brajša, R., Wöhl, H., Vršnak, B., et al. 2001a, A&A, 374, 309 (Paper I)
Brajša, R., Wöhl, H., Schuck, T. J., et al. 2001b, Hvar Obs. Bull., 25, 13 (Paper II)
Brajša, R., Wöhl, H., Vršnak, B., et al. 2002, Sol. Phys., 206, 229
Brković, A., Solanki, S. K., & Rüedi, I. 2001, A&A, 373, 1056
Brown, D. S., Parnell, C. E., DeLuca, E. E., Golub, L., & McMullen, R. A. 2001, Sol. Phys., 201, 305
Carbonell, M., Oliver, R., & Ballester, J. L. 1993, A&A, 274, 497
Chertok, I. M. 1999, Proc. 8th SOHO Workshop, ESA SP-446, 229
Chertok, I. M. 2001, Sol. Phys., 198, 367
Gaizauskas, V., Harvey, K. L., Harvey, J. W., & Zwaan, C. 1983, ApJ, 265, 1056
Golub, L., & Pasachoff, J. M. 1997, The Solar Corona (Cambridge University Press, Cambridge), 190
Golub, L., Krieger, A. S., Silk, J. K., Timothy, A. F., & Vaiana, G. S. 1974, ApJ, 189, L93
Harvey-Angle, K. L. 1993, Magnetic Bipoles on the Sun, Ph.D. Thesis, University of Utrecht
Hoeksema, J. T., & Scherrer, P. H. 1987, ApJ, 318, 428
Koutchmy, S., Hara, H., Suematsu, Y., & Reardon, K. 1997, A&A, 320, L33
Krucker, S., Benz, A. O., Bastian, T. S., & Acton, L. W. 1997, ApJ, 488, 499
Nash, A. G. 1991, ApJ, 366, 592
Nash, A. G., Sheeley, N. R. Jr., & Wang, Y.-M. 1988, Sol. Phys., 117, 359
Oliver, R., & Ballester, J. L. 1994, Sol. Phys., 152, 481
Roša, D., Brajša, R., Vršnak, B., & Wöhl, H. 1995, Sol. Phys., 159, 393
Sheeley, N. R. Jr., Nash, A. G., & Wang, Y.-M. 1987, ApJ, 319, 481
Shimizu, T., Tsuneta, S., Acton, L. W., et al. 1994, ApJ, 422, 906
Stix, M. 1989, The Sun (Springer-Verlag, Berlin), 239
Vernova, E. S., Mursula, K., Tyasto, M. I., & Baranov, D. G. 2002, Sol. Phys., 205, 371
Vršnak, B., Roša, D., Božić, H., et al. 1999, Sol. Phys., 185, 207
Wang, Y.-M., & Sheeley, N. R. Jr. 1994, ApJ, 430, 399
Wöhl, H., Brajša, R., Vršnak, B., et al. 2001, Hvar Obs. Bull., 25, 27 (Paper III)